

Supplementary Information for

A remote input of African dust to Last Glacial Europe

Authors: Denis-Didier Rousseau^{1,2,3*}, Catherine Chauvel⁴, Peter O Hopcroft⁵, Pamela Gutiérrez⁴, Ségolène Saulnier-Copard⁶, Pierre Antoine⁶, Markus Fuchs⁷, and Alicja Ustrzycka²

Affiliations:

¹Géosciences Montpellier, Université de Montpellier, Montpellier, cedex05, France

²Institute of Physics-CSE, Division of Geochronology and Environmental Isotopes, Silesian University of Technology, Gliwice, 44-100, Poland

³Lamont Doherty Earth Observatory, Columbia University, Palisades, NY10964, USA

⁴Université Paris Cité, Institut de Physique du Globe de Paris, CNRS, F-75005 Paris, France

⁵School of Geography, Earth & Environmental Sciences, University of Birmingham, Birmingham B15 2TT, UK

⁶Laboratoire de Géographie Physique, Université Paris 1, Thiais, France

⁷Department of Geography, Justus Liebig-University Giessen, 35390 Giessen Germany

*Corresponding author. Email: denis-didier.rousseau@umontpellier.fr

Supplementary Materials include:

Supplementary Figures 1-4

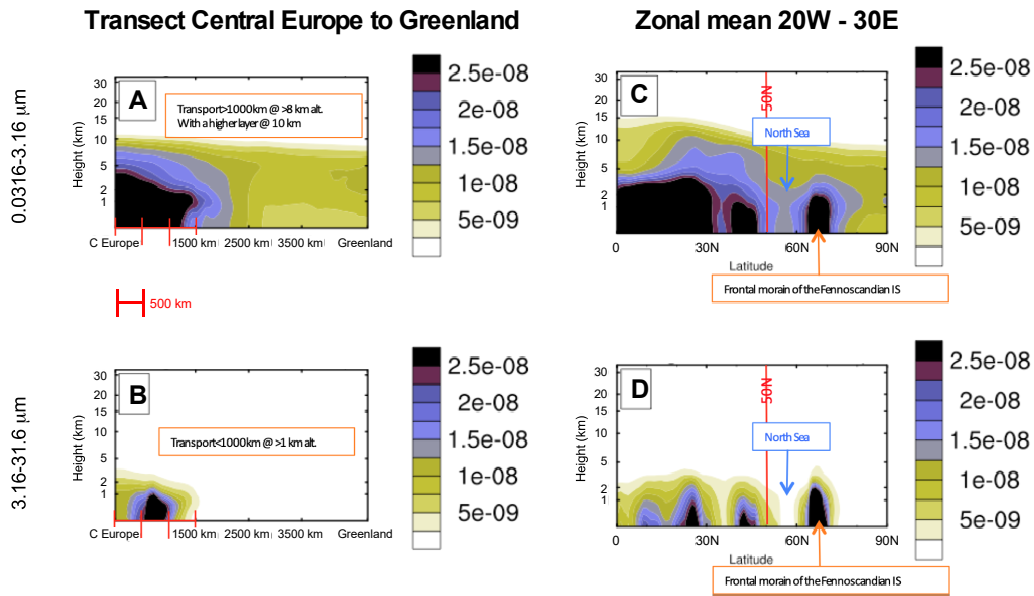
Supplementary Tables 1-3

Supplementary Data File 1

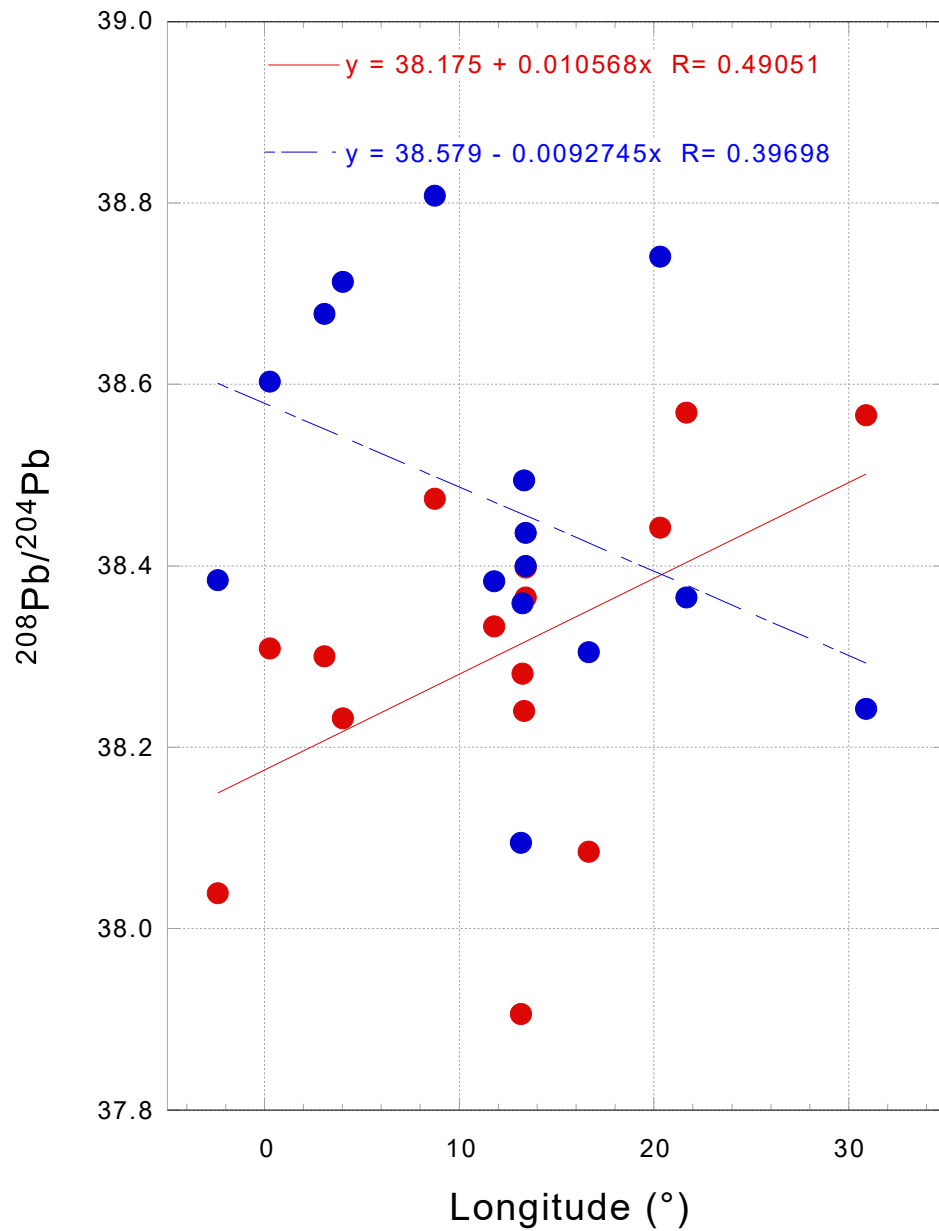
References

Data and materials availability: In addition to the new data produced in this study, we used published data listed in the references. The data that supports the findings of this study are provided in the Supplementary Tables and are openly available in the open access PANGAEA Data Repository [1](#).

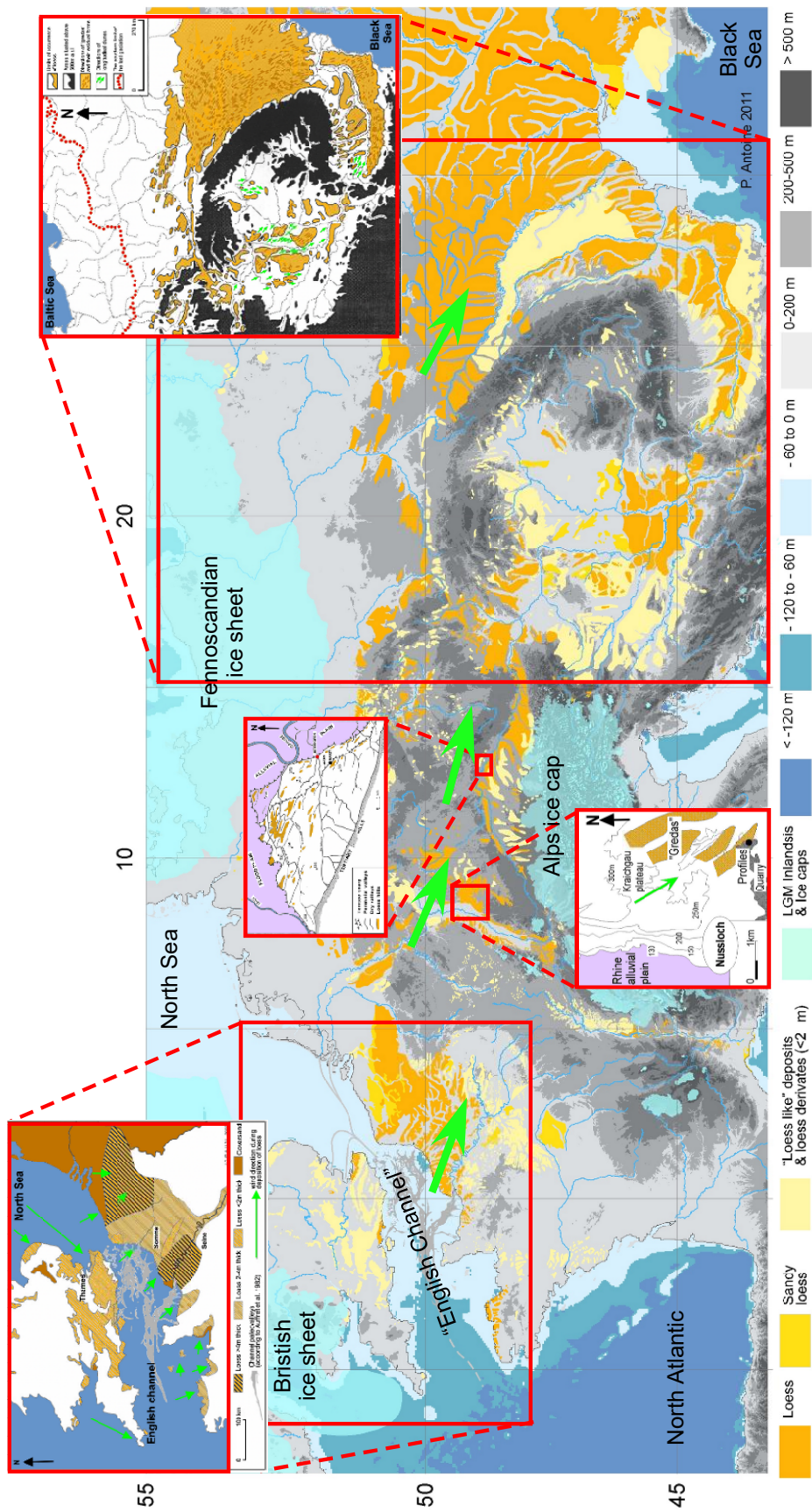
Supplementary Figures



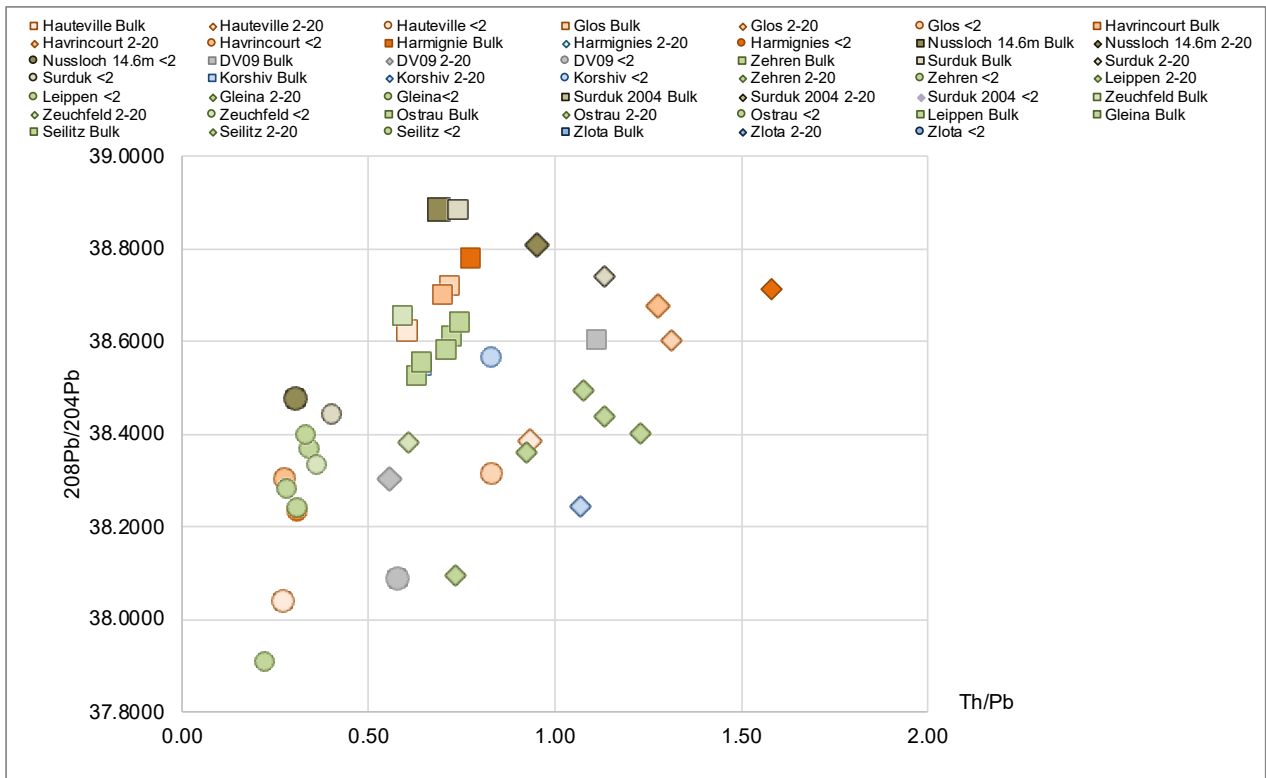
Supplementary Figure 1. Dust loadings in kg/kg in LGM simulation (with glaciogenic sources + 1.0Sv freshwater forcing in the Atlantic) from Hopcroft et al. ² for two grain size10 fractions. On the left, transect from Central Europe to Greenland. On the right, zonal mean from 20W to 30E. A and C fraction 0.0316 to 3.16 μm ; B and D fraction 3.16 and 31.6 μm .



Supplementary Figure 2. Plot of $^{208}\text{Pb}/^{204}\text{Pb}$ ratios of European loess samples as a function of longitude. The <2 μm grain size fractions are shown in red and the 2-20 μm fractions in blue. Linear regressions for both groups are also shown.



Supplementary Figure 3. Map of European loess showing main wind directions deduced from loess deposits geomorphology and mineral contents in Western Europe³, Rhine valley⁴, Bavaria⁵, and eastern Europe⁶



Supplementary Figure 4. $^{208}\text{Pb}/^{204}\text{Pb}$ vs Th/Pb plot showing the isotopic variability among the three grain-size fractions of the studied European loess. The figure illustrates that the difference between fine and coarse fractions cannot be explained by simple mineral sorting processes. In such sedimentary material, the Th/Pb and $^{208}\text{Pb}/^{204}\text{Pb}$ ratios are primarily controlled by the proportion of monazite (Garçon et al., 2014⁷). If mineral sorting was the sole active process explaining the difference between monazite-poor fine fractions and monazite-rich coarse fractions, the values measured for the bulks should be intermediate between the two and it is not the case.

Supplementary Tables

Supplementary Table 1. Sites location and code

Sequence	Code	Long. (°)	Lat. (°)	Country	Age	Reference
La Hauteville	HV	-1.87	48.65	France	21±2 ka OSL	Antoine, unpublished report
Glos	GL	0.28	49.01		±25 ka strati	Lautridou (1985) ⁸
Havrincourt	HR	3.08	50.12		28.3 ka OSL	Antoine et al. (2014) ⁹
Harmignies	HA	4.02	50.41	Belgium	20-24 ka TL	Haesaerts et al. (2016) ¹⁰
Nussloch	NU	8.73	49.32	Germany	19±3 ka OSL	Antoine et al. (2009) ¹¹
Zeuchfeld	ZE	11.8	51.23		22.5 ka 14C Gr ±20 ka strati	Moine et al. (2017) ¹² Meszner et al. (2011, 2013) ^{13,14}
Ostrau	OS	13.18	51.2		20.4±2.8-22.3±3.0 ka OSL	Meszner et al. (2013) ¹⁴
Gleina	GE	13.24	51.23		±20 ka strati	Meszner et al. (2011, 2013) ^{13,14}
Leippen	LE	13.33	51.13		±20 ka strati	Meszner et al. (2011, 2013) ^{13,14}
Seilitz	SE	13.40	51.19		20.4±2.1-21.7±2.8 ka OSL	Meszner et al. (2013) ¹⁴
Zehren	ZH	13.4	51.2		±20 ka strati	Meszner et al. (2011, 2013) ^{13,14}
Dolni Vestonice	DV	16.65	48.88	Czech Republic	±20 ka strati	Antoine et al. (2013) ¹⁵ Fuchs et al. (2013) ¹⁶
Surduk	SU	20.33	45.07	Serbia	±20 ka strati	Antoine et al. (2009) ¹⁷ Fuchs et al. (2008) ¹⁸
Zlota	ZL	21.65	50.65	Poland	20-23 ka OSL	Moska et al. (2018) ¹⁹
Korshiv	KO	25.16	50.64	Ukraine	19.2-22.5 ka OSL	Fedorowicz et al. (2013) ²⁰

Supplementary Table 2. Percentages of the four different grain-size fractions separated from the studied European LGM loess samples.

Ⓜ

Sites	Grain-size fractions (μm)			
	< 2	2-20	20-63	> 63
Dolni Vestonice (CZE)	18.92	12.03	29.44	38.70
Gleina (DEU)	17.36	21.76	54.93	5.83
Glos (FRA)	23.36	23.88	45.25	2.30
Harmignies (BEL)	16.99	17.77	62.73	1.61
Havrincourt (FRA)	20.10	23.58	54.77	0.69
Korshiv (UKR)	26.78	31.23	38.13	3.00
La Hauteville (FRA)	14.66	15.03	64.98	4.69
Leippen (DEU)	20.13	27.44	51.27	1.45
Nussloch (DEU)	10.01	19.55	61.89	6.74
Ostrau (DEU)	17.38	23.93	55.76	3.00
Seilitz (DEU)	17.99	33.35	43.10	2.06
Surduk (SRB)	29.54	21.80	40.86	6.14
Surduk (SRB)	21.58	27.97	45.78	3.34
Zehren (DEU)	16.46	21.49	57.70	3.81
Zeuchfeld (DEU)	19.67	27.09	42.00	9.88
Zlota (POL)	19.30	25.87	51.89	2.66

mean =	19.39	23.36	50.03	5.99
sd =	4.58	5.61	9.91	9.04

Ⓜ

Supplementary Table 3. Summary of restricted emissions area simulations with HadGEM2. The regional contributions show how much of the total dust can be attributed to each source region

Simulation	Emission region(s)	Fine dust flux (<0.316 μm) Europe: 20 °W-30 °E by 47.5-52.5 °N	Fine particle regional contribution	Coarse dust flux (>3.16 μm) Europe: 20 °W-30 °E by 47.5-52.5 °N	Coarse particle regional contribution
		[g m ⁻² a ⁻¹]	[%]	[g m ⁻² a ⁻¹]	[%]
LGM	Globe	0.22	-	0.8	-
	Africa	0.15	66	0.90	~100
	Atlantic region	0.17	75	0.94	~100
	Asia	0.04	18	0.01	1.3
LGMglac	Globe	0.34	-	67.4	-
	Africa	0.15	43	0.94	1.4
	Atlantic region	0.19	55	0.97	1.4
	Asia	0.04	11	0.01	0.01
LGMglac+fw1	Globe	0.42	-	122	
	Africa	0.16	38	0.91	0.75
	Atlantic region	0.18	42	0.87	0.71
	Asia	0.085	22	0.065	0.05

Supplementary references

1. Rousseau, D.-D. *et al.* Geochemical signature of last glacial maximum European loess samples [dataset bundled publication]. PANGAEA <https://doi.org/10.1594/PANGAEA.971902> (2024).
2. Hopcroft, P. O., Pichat, S., Valdes, P. J. & Kienast, S. S. Sensitivity of the tropical dust cycle to glacial abrupt climate changes. *Geophys. Res. Lett.* **50**, e2022GL101197 (2023).
3. Antoine, P., Catt, J., Lautridou, J. P. & Somme, J. The loess and coversands of northern France and southern England. *J. Quat. Sci.* **18**, 309–318 (2003).
4. Antoine, P. *et al.* High-resolution record of the last interglacial-glacial cycle in the nussloch loess-palaeosol sequences, upper rhine area, Germany. *Quat. Int.* **76–77**, 211–229 (2001).
5. Léger, M. Loess Landforms. *Quat. Int.* **7/8**, 53–61 (1990).
6. Rozycki, S. Z. Le sens des vents portant la poussière de loess à la lumière de l'analyse des formes d'accumulation du loess en Bulgarie et en Europe Centrale. *Rev. Geomorphol. Dyn.* **1**, 1–9 (1967).
7. Garçon, M., Chauvel, C., France-Lanord, C., Limonta, M. & Garzanti, E. Which minerals control the Nd–Hf–Sr–Pb isotopic compositions of river sediments? *Chem. Geol.* **364**, 42–55 (2014).
8. Lautridou, J.-P. Le cycle périglaciaire pléistocène en Europe du Nord-Ouest et plus particulièrement en Normandie. (Université de Caen, Centre de Géomorphologie, 1985).
9. Antoine, P. *et al.* Les séquences loessiques pléistocène supérieur d'Havrincourt (Pas-de-Calais, France): stratigraphie, paléoenvironnements, géochronologie et occupations paléolithiques. *Quaternaire* **25**, 321–368 (2014).
10. Haesaerts, P., Damblon, F., Gerasimenko, N., Spagna, P. & Pirson, S. The Late Pleistocene loess-palaeosol sequence of middle Belgium. *Quat. Int.* **411**, 25–43 (2016).
11. Antoine, P. *et al.* Rapid and cyclic aeolian deposition during the Last Glacial in European loess: a high-resolution record from Nussloch, Germany. *Quat. Sci. Rev.* **28**, 2955–2973 (2009).
12. Moine, O. *et al.* The impact of Last Glacial climate variability in west-European loess revealed by radiocarbon dating of fossil earthworm granules. *Proc. Natl. Acad. Sci. USA.* **114**, 6209–6214 (2017).
13. Meszner, S., Fuchs, M. & Faust, D. Loess-Palaeosol-Sequences from the loess area of Saxony (Germany). *E&Q Quat. Sci. J.* **60**, 4 (2011).
14. Meszner, S., Kreutzer, S., Fuchs, M. & Faust, D. Late Pleistocene landscape dynamics in Saxony, Germany: Paleoenvironmental reconstruction using loess-paleosol sequences. *Quaternary International* **296**, 94–107 (2013).
15. Antoine, P. *et al.* High-resolution record of the environmental response to climatic variations during the Last Interglacial-Glacial cycle in Central Europe: The loess-palaeosol sequence of Dolní Věstonice (Czech Republic). *Quat. Sci. Rev.* **67**, 17–38 (2013).
16. Fuchs, M. *et al.* The loess sequence of Dolní Věstonice, Czech Republic: A new OSL-based chronology of the Last Climatic Cycle. *Boreas* **42**, 664–677 (2013).
17. Antoine, P. *et al.* High-resolution record of the last climatic cycle in the southern Carpathian Basin (Surduk, Vojvodina, Serbia). *Quat. Int.* **198**, 19–36 (2009).
18. Fuchs, M. *et al.* Chronology of the Last Climatic Cycle (Upper Pleistocene) of the Surduk loess sequence, Vojvodina, Serbia. *Boreas* **37**, 66–73 (2008).
19. Moska, P. *et al.* Luminescence chronostratigraphy for the loess deposits in Złota, Poland. *Geochronometria* **45**, 44–55 (2018).
20. Fedorowicz, S. *et al.* Loess-paleosol sequence at Korshiv (Ukraine): Chronology based on complementary and parallel dating (TL, OSL), and litho-pedosedimentary analyses. *Quat. Int.* **296**, 117–130 (2013).